WILEY-VCH

UNIVERSITÀ DEGLI STUDI DI TORINO

***This is an author version of the contribution published on:***

Dario L. Longo, Rachele Stefania, Chiara Callari, Francesco De Rose, Riccardo Rolle, Laura Conti, Lorena Consolino, Francesca Arena, and Silvio Aime

Water Soluble Melanin Derivatives for Dynamic Contrast Enhanced Photoacoustic Imaging of Tumor Vasculature and Response to Antiangiogenic Therapy

In ADVANCED HEALTHCARE MATERIALS 2017, 6, 1600550

***The definitive version is available at:***

***DOI:*** 10.1002/adhm.201600550

DOI: 10.1002/adma.((please add manuscript number))
**Article type: Communication**

# Water Soluble Melanin Derivatives for Dynamic Contrast Enhanced Photoacoustic Imaging of Tumor Vasculature and Response to Antiangiogenic Therapy

By *Dario L. Longo, Rachele Stefania, Chiara Callari, Francesco De Rose, Riccardo Rolle, Laura Conti, Lorena Consolino, Francesca Arena,* and *Silvio Aime**

Prof. S. Aime, Dr. R. Stefania, C. Callari, Dr. F. De Rose, Dr. R. Rolle, Dr. L. Conti, Dr. L. Consolino, Dr. F. Arena
Department of Molecular Biotechnology and Health Sciences, University of Torino
Via Nizza 52, 10126 Torino, Italy
E-mail: silvio.aime@unito.it
Dr. D.L. Longo
Institute of Biostructure and Bioimaging (CNR) c/o Molecular Biotechnologies Center
Via Nizza 52, 10126, Torino, Italy

Keywords: nanoparticles; photoacoustic; melanin; dynamic contrast enhanced; tumor

Recent advances in nanobiotechnology and nanomaterials are providing novel functional agents that hold great potential in several imaging-based approaches for cancer diagnosis and therapy.[1] Photoacoustic (PA) imaging is a hybrid imaging technique for non invasive visualization of tissue structures that combine optical excitation with ultrasound detection, exploiting the PA effect.[2] Thanks to the high spatial resolution and imaging depth that this modality can provide, the endogenous PA contrast from naturally occurring tissue cromophores, such as hemoglobin and melanin, allows monitoring anatomic and physiological changes in several diseases as well as following treatment response.[3] Notably, photoacoustic imaging has already been exploited for visualizing human breast cancer based on the intrinsic optical absorption contrast.[4] However, intrinsic PA contrast is usually small

and this has prompted the search for exogenous contrast (e.g. organic dyes, quantum dots, carbon nanotubes, gold nanorods and other platforms) to enhance the role of this imaging modality as diagnostic tool.[5] It has been shown that these agents may markedly improve resolution and sensitivity of PA imaging and the quest for novel materials with improved optoacoustic properties, optimal biodistribution and low cytotoxicity continues to be under intense scrutiny to expand PA imaging applications.[6] In this context, materials based on naturally occurring biomolecules are receiving great attention due to the obvious biocompatibility they may offer.

Here, we report a novel melanin-based PA contrast agent, as an efficient probe for assessing tumor vasculature properties that allows, for the first time, the set-up of a Dynamic Contrast Enhanced (DCE)-PA approach to monitor vascular changes following an anti-angiogenic treatment.

Melanin is a natural pigment found widespread in nature including human skin. Dark-brown melanin, or eumelanin, is a macromolecular insoluble structure formed by high-molecular weight polymeric chains with a broad set of biological functions, remarkable for their protective role in oxidative stress, as anti-oxidant, free radical scavenger and metal ion storage.[7] Moreover, the broad absorption spectrum of melanin and its good stability in physiological environments makes it well suitable for PA imaging in live animals.[8] Recently, PA probes based on melanin-like nanoparticles have been proposed. These nanoparticles were prepared from synthetic melanin granules dissolved in basic conditions and sonicated to limit aggregation (i.e. to improve their dispersion in aqueous solutions) or by synthesis of artificial melanin models from chemical oxidation of dopamine followed by linear polymerization.[9] As recently pointed out, the capability to control the aggregation state of melanin and hence its solubility is essential for future developments of melanin as functional materials within the PA field.[10] Importantly, melanin-containing nanoparticles can be exploited for multimodality imaging, owing to ability of the melanin macromolecules to chelate metal ions, as well as for

drug-loading systems due to its binding capabilities through electrostatic and π-π interactions.[11] However, the aforementioned methods have some limitations associated to the fact that sonication of the melanin granules often results in a marked degradation of the original structure. Therefore we adopted a novel strategy for obtaining water soluble melanin derivatives that retain the melanin properties, with dimensions that are optimal in term of pharmacokinetic and biodistribution within tumors.

Importantly, exogenous agents are commonly exploited in several imaging modalities for assessing tumor microvasculature properties. Dynamic Contrast Enhanced (DCE) imaging is a well established technique that describes the acquisition of baseline images followed by a series of images acquired over time after the intravenous administration of a contrast agent.[12] The characteristic wash-in and wash-out enhancement curves of the contrast agent provide information on the tumor vascular compartment. Notably, DCE is a useful tool for providing early measurement of vascular functional changes after therapeutic treatment and therefore it is considered as a useful biomarker of drug treatment response.[13] In addition, agents with size close to serum albumin can provide a better assessment of tumor vessel permeability and monitor more precisely changes upon anti-angiogenic treatment.[14]

In this study, we prepared highly water soluble Melanin Free-Acid (MFA) starting from synthetic melanin granules (sMG) through a slight modified “bleaching” procedure (**Figure 1a)**. sMG were synthesized by enzymatic (tyrosinase) oxidation of L-dopa.[15] Solubilization of sMG is typically achieved by treatment with hydrogen peroxide in alkaline solution.[16] To remove the solubility-restraining crosslinks but still preserving the overall chemical nature of the pigment, we applied a light oxidative breakdown of the melanin structure under mild and neutral pH conditions for a short period of time. Briefly, synthetic sMG were treated with 0.3 M $H_2O_2$ in 0.12 M ammonia buffer at pH 7 for 20 min at 30 °C. After this mild treatment, the solution phase became dark colored because of the partial solubilization of sMG to yield the MFA derivative (**Figure 1a** and **1b**).

The obtained MFA exhibited excellent stability and water solubility up to 10 mg/ml, with no precipitation after storage at 4°C for several months (**Figure 1b**). To further improve dispersibility for applications in living animals, polyethylene glycol (PEG-3000) chains were conjugated to MFA. The MFA-PEG derivative (**Figure 1b**) has been obtained by a cross-linking reaction between the amine groups of $NH_2$-$PEG_{3000}$-$NH_2$ and the carboxylic groups of MFA. Purification was carried out by gel-filtration chromatography on a Superdex 200 10/300 GL column. The ratio of PEG chains per MFA molecule was determined to be 3:1 by $^1$H NMR spectroscopy using sodium 3-(trimethylsilyl)propionate-2,2,3,3-d4 as internal standard (data not shown). The obtained MFA-PEG derivatives maintained the brown-to-black color of the parent MFA (**Figure 1b**).

Dynamic light scattering data showed an average diameter of 6.9 ± 1.2 nm for MFA that reached 10.5 ± 1.8 nm for the PEG-functionalized MFA (**Figure S1**). The size of the synthesized MFA derivatives appears slightly smaller than that of natural occurring melanin, which is 20-300 nm in diameter and spherical in shape.[17] From the point of view of a biological application, small-size systems are expected to be more suitable for biological applications than larger particles, because they are less likely to be rapidly recognized and cleared by macrophages by complement receptor-mediated phagocytosis and they can more easily avoid cellular internalization. [18] The similar absorption spectrum of MFA-PEG and MFA demonstrated that the PEG-modification did not influence the absorption properties of MFA and that both MFA and MFA-PEG possess similar optical properties as the parent melanin (**Figure 1c**).[17]

Stability of MFA nanoparticles in water was assessed by DLS measurements over a period of 3 months, with no changes in size (**Figure S2**). The physiological stability of MFA and MFA-PEG was assessed in cell culture medium (DMEM) and in PBS added of 10% fetal bovine serum, at 37°C. No changes in PA properties and in absorbance at 700nm were observed after incubation up to 24h in both media (**Figure S3** and **S4**, respectively). These data suggest that

both MFA and MFA-PEG hold a good chemical and physiological stability and are therefore suitable for *in vivo* applications.

To assess the potential of MFA and MFA-PEG to be used as PA agents, we investigated the detection sensitivity of their aqueous solutions at increasing concentration, from 0.6 to 2.5 mg/ml. The PA signal increased with the concentration of the MFA and MFA-PEG, with MFA-PEG invariantly showing higher optoacoustic signal intensities at all the investigated wavelengths (**Figure 1d**). MFA and MFA-PEG yield the best PA response, with maximum ultrasound emission, upon excitation at ca. 700 nm value. This wavelength appears well suitable for *in vivo* work due to the low absorption of de-oxygenated blood at this wavelength. In fact, the PA signal generated at ca. 700 nm by a blood sample added of 1.25 mg/ml MFA and MFA-PEG, respectively, was significantly higher of the one obtained from the neat blood, as shown in **Figure S4**. At higher excitation wavelengths, the MFA containing phantoms display lower PA responses, in comparison to the pure blood sample, reflecting the low PA efficiency of MFA and MFA-PEG at wavelength exceeding 750 nm (**Figure 1d**). At 700 nm both MFA and MFA-PEG displayed a linear relationship between PA signal and concentrations (R2 = 0.996 and 0.987 for MFA and MFA-PEG, respectively, **Figure 1e**). The PA intensity is overlaid with the ultrasound image in **Figure 1f**, to obtain a tomographic composite image, displaying higher intensities for the MFA-PEG compound.

Tissue culture experiments were used in vitro for pilot toxicity studies. The MFA and MFA-PEG were first tested with J774 macrophage cells plated in 96 well plates. Increasing concentrations of MFA and MFA-PEG were added to the culture media and allowed to incubate for 24 h. Analysis with the MTT viability assay indicated no statistically significant decrease in cell viability even at highest concentrations of 2.5 mg/ml, for both MFA and MFA-PEG (**Figure S5**).

The biodistribution of MFA-PEG was carried out in BALB/c mice bearing a subcutaneous HER2 positive breast tumor generated by injection of ca. $2.5 \cdot 10^5$ TS/A cells. All animal

experiments were performed complying with the EU guidelines for the care and use of laboratory animals and with our University Ethical committee's requirements and according to a protocol approved by the Institutional animal care. Mice were injected intravenously with MFA-PEG labeled with a fluorescent dye (S-07186, Ferrania Technologies, Italy), named MFA-PEG-Cy5 (25 µl of 0.06 mM MFA-PEG-Cy5 solution) that shows a fluorescence emission peak at 660-670 nm (**Figure S6**). The dynamic optical imaging data revealed a rapid distribution and elimination of MFA-PEG-Cy5 in the tumor. Indeed, fluorescent intensity in the tumor reached a high level in the first 5 min after injection of MFA-PEG-Cy5 up to 30 min, followed by a quite fast wash-out (**Figure S7**). MFA-PEG-Cy5 showed a good selectivity in the tumor as a significantly lower signal was detected in the muscle at all time points (**Figure S7**). *Ex-vivo* evaluation of organs 4 h post injection clearly showed that the highest fluorescence emission was associated with the tumor tissue. MFA-PEG-Cy5 was also found in the liver and the kidneys, the main organs involved in the elimination of the compound, while no specific signal was detected in the heart, lung, spleen and muscle. In all the organs explanted from control mice treated with the unlabeled compound a low signal, caused by tissue autofluorescence, was observed (**Figure S8**). The capability of MFA and MFA-PEG for tumor imaging was validated by performing *in vivo* PA imaging in the HER2 positive TS/A tumor model. Three groups of mice (n=4 for each group) received intravenous administration of 100 µL of a saline solution, or of MFA and MFA-PEG solutions with concentration of 2.5 mg/mL. After systemic administration of MFA, the PA signal in the tumor gradually increased during the first 30 min, in analogy to what observed in the optical imaging experiments. The average increase, upon subtraction of the baseline PA signal, was in the range 0.05-0.10 a.u. (**Figure 2a**). Upon the systemic administration of MFA-PEG at the same dose, a marked and higher increase of the PA signal was observed in the tumor area, with an average increase between 0.10-0.20 a.u. (**Figure 2b**). The higher contrast enhancement obtained for the MFA-PEG solution likely reflects the enhanced optoacoustic

properties of the MFA-PEG in comparison to the MFA compound. Pre-contrast PA images showed weak PA response in the region of interest, essentially due to the intrinsic absorption of oxyhemoglobin and deoxyhemoglobin in the NIR region (**Figure 2d**, **2e** and **2f**). PA images overimposed onto the B-mode images showed a heterogeneous distribution of the signal, with a slight prevalence in the rim region in comparison to the core area (**Figure 2d** and **2e**). The good PA contrast generated by MFA and MFA-PEG can be accounted in terms of the enhanced permeability and retention (EPR) effect within tumors. The administration to the control group of the saline solution did not increase at all the PA signal in the first 15 min, with a successive slight reduction (**Figure 2c** and **2f**). These results give support to the view that the enhanced PA signal in tumor is due to the passive extravasation and accumulation of the MFA and MFA-PEG derivatives.

A further step in tumor characterization is represented by the assessment of tumor vascular permeability. To examine the ability to visualize dynamically tumor vessel permeability, a DCE-PA imaging experiment was performed upon the injection of MFA-PEG into the tail vein. The uptake of MFA-PEG over time was monitored within the tumor region, from which time-intensity PA signal can be extracted and used to describe the microvasculature features (**Figure 3a**). The DCE-PA curve showed a slow but constant uptake into the tumor up to 15 min post-injection. Additionally, to validate the DCE-PA approach for assessing changes in tumor vascularization, we treated a group of mice with tumor necrosis factor-α (TNF-α), an agent used in clinical trials known to increase vascular permeability and uptake of nano-sized systems into tumors [19]. Thus, we carried DCE-PA imaging on mice bearing subcutaneous TS/A tumors after intravenous injection of saline solution or of TNF-α. Post-treatment images were acquired after 3 h to allow sufficient time for tumors to respond to TNF-α treatment.[20] Averaged DCE-PA time curves are shown in **Figure 3b** for control and TNF-α treated group, respectively. As compared to the control group, the PA enhancement curve for the TNF-α group significantly increased upon time after the MFA-PEG injection. To quantify the

differences between the two groups, we calculated the area under the curve (AUC) at several time points from the DCE-PA curves. A relatively small increase in AUC values was observed up to 6 min post injection, which significantly increased from 8 to 12 min (**Figure 3c**). Clearly the DCE-PA imaging demonstrated that the increase of PA contrast is specific for the enhanced accumulation of MFA-PEG molecules in tumors due to the TNF-α treatment.

In conclusion, we have reported a new synthetic way to produce melanin-based nanosized systems possessing high water solubility as an active platform for PA imaging. These PA nanoscale agents possess relatively small size, good optoacoustic properties and excellent biocompatibility that point to their use as passive tumor targeting agents. Moreover, for the first time, we showed that these agents can be exploited within a DCE-PA approach for the assessment of changes in tumor vasculature after treatment. In addition, owing to the presence of amine moieties on the surface of these particles, one can envisage to exploit these anchoring points for the conjugation of suitable vectors for *in vivo* active targeting of specific molecular markers.[21]

**Supporting Information**

Experimental details and Figures S1-S8 are included in the Supporting Information.
Supporting Information is available online from Wiley InterScience or from the author.

**Acknowledgements**

Received: ((will be filled in by the editorial staff))
Revised: ((will be filled in by the editorial staff))
Published online: ((will be filled in by the editorial staff))

**References**

[1] K. T. Yong, I. Roy, M. T. Swihart, P. N. Prasad, *J Mater Chem* **2009**, *19*, 4655; Y. Liu, H. Miyoshi, M. Nakamura, *Int J Cancer* **2007**, *120*, 2527; I. Brigger, C. Dubernet, P. Couvreur, *Adv Drug Deliv Rev* **2002**, *54*, 631; W. H. Chen, C. X. Yang, W. X. Qiu, G. F. Luo, H. Z. Jia, Q. Lei, X. Y. Wang, G. Liu, R. X. Zhuo, X. Z. Zhang, *Adv Healthc Mater* **2015**, *4*, 2247.

[2] R. A. Kruger, P. Liu, Y. R. Fang, C. R. Appledorn, *Med Phys* **1995**, *22*, 1605; V. Ntziachristos, D. Razansky, *Chem Rev* **2010**, *110*, 2783; L. V. Wang, S. Hu, *Science* **2012**, *335*, 1458; R. Su, S. Ermilov, A. Liopo, A. Oraevsky, *Nucl Instrum Methods Phys Res A* **2013**, *720*, 58; V. Ntziachristos, D. Razansky, *Recent Results Cancer Res* **2013**, *187*, 133.

[3] J. Yao, L. V. Wang, *Contrast Media Mol Imaging* **2011**, *6*, 332; J. Laufer, P. Johnson, E. Zhang, B. Treeby, B. Cox, B. Pedley, P. Beard, *J Biomed Opt* **2012**, *17*, 056016; S. E. Bohndiek, L. S. Sasportas, S. Machtaler, J. V. Jokerst, S. Hori, S. S. Gambhir, *J Nucl Med* **2015**, *56*, 1942.

[4] J. Menke, *Eur Radiol* **2015**, *25*, 2205; Z. Xie, F. M. Hooi, J. B. Fowlkes, R. W. Pinsky, X. Wang, P. L. Carson, *Ultrasound Med Biol* **2013**, *39*, 2176; M. Schwarz, A. Buehler, J. Aguirre, V. Ntziachristos, *J Biophotonics* **2016**, *9*, 55; S. Manohar, S. E. Vaartjes, J. C. G. van Hespen, J. M. Klaase, F. M. van den Engh, W. Steenbergen, T. G. van Leeuwen, *Optics Express* **2007**, *15*, 12277.

[5] G. P. Luke, D. Yeager, S. Y. Emelianov, *Ann Biomed Eng* **2012**, *40*, 422; A. De la Zerda, C. Zavaleta, S. Keren, S. Vaithilingam, S. Bodapati, Z. Liu, J. Levi, B. R. Smith, T. J. Ma, O. Oralkan, Z. Cheng, X. Chen, H. Dai, B. T. Khuri-Yakub, S. S. Gambhir, *Nat Nanotechnol* **2008**, *3*, 557; G. Ku, M. Zhou, S. Song, Q. Huang, J. Hazle, C. Li, *ACS Nano* **2012**, *6*, 7489; J. Levi, S. R. Kothapalli, T. J. Ma, K. Hartman, B. T. Khuri-Yakub, S. S. Gambhir, *J Am Chem Soc* **2010**, *132*, 11264; A. V. Liopo, A. Conjusteau, O. V. Chumakova,

S. A. Ermilov, R. Su, A. A. Oraevsky, *Nanosci Nanotechnol Lett* **2012**, *4*, 681; R. Su, S. A. Ermilov, A. V. Liopo, A. A. Oraevsky, *J Biomed Opt* **2012**, *17*, 101506.

[6] K. Pu, J. Mei, J. V. Jokerst, G. Hong, A. L. Antaris, N. Chattopadhyay, A. J. Shuhendler, T. Kurosawa, Y. Zhou, S. S. Gambhir, Z. Bao, J. Rao, *Adv Mater* **2015**, *27*, 5184; D. Zhang, G. B. Qi, Y. X. Zhao, S. L. Qiao, C. Yang, H. Wang, *Adv Mater* **2015**, *27*, 6125; X. Zhu, H. Wang, L. Zheng, Z. Zhong, X. Li, J. Zhao, J. Kou, Y. Jiang, X. Zheng, Z. Liu, H. Li, W. Cao, Y. Tian, Y. Wang, L. Yang, *Int J Nanomedicine* **2015**, *10*, 3719; E. V. Petrova, A. A. Oraevsky, S. A. Ermilov, *Appl Phys Lett* **2014**, *105*, 094103; S. Manohar, C. Ungureanu, T. G. Van Leeuwen, *Contrast Media Mol Imaging* **2011**, *6*, 389; J. Zeng, M. Cheng, Y. Wang, L. Wen, L. Chen, Z. Li, Y. Wu, M. Gao, Z. Chai, *Adv Healthc Mater* **2016**, *5*, 772.

[7] F. P. Noonan, M. R. Zaidi, A. Wolnicka-Glubisz, M. R. Anver, J. Bahn, A. Wielgus, J. Cadet, T. Douki, S. Mouret, M. A. Tucker, A. Popratiloff, G. Merlino, E. C. De Fabo, *Nat Commun* **2012**, *3*, 884; J. Sedo, J. Saiz-Poseu, F. Busque, D. Ruiz-Molina, *Advanced Materials* **2013**, *25*, 653.

[8] J. B. Dawson, D. J. Barker, D. J. Ellis, E. Grassam, J. A. Cotterill, G. W. Fisher, J. W. Feather, *Phys Med Biol* **1980**, *25*, 695; J. Stritzker, L. Kirscher, M. Scadeng, N. C. Deliolanis, S. Morscher, P. Symvoulidis, K. Schaefer, Q. Zhang, L. Buckel, M. Hess, U. Donat, W. G. Bradley, V. Ntziachristos, A. A. Szalay, *Proc Natl Acad Sci U S A* **2013**, *110*, 3316; C. X. Qin, K. Cheng, K. Chen, X. Hu, Y. Liu, X. L. Lan, Y. X. Zhang, H. G. Liu, Y. D. Xu, L. H. Bu, X. H. Su, X. H. Zhu, S. X. Meng, Z. Cheng, *Scientific Reports* **2013**, *3*.

[9] T. Repenko, S. Fokong, L. De Laporte, D. Go, F. Kiessling, T. Lammers, A. J. Kuehne, *Chem Commun (Camb)* **2015**, *51*, 6084; A. Liopo, R. Su, A. A. Oraevsky, *Photoacoustics* **2015**, *3*, 35; Q. Fan, K. Cheng, X. Hu, X. Ma, R. Zhang, M. Yang, X. Lu, L. Xing, W. Huang, S. S. Gambhir, Z. Cheng, *J Am Chem Soc* **2014**, *136*, 15185.

[10] G. Greco, L. Panzella, G. Gentile, M. E. Errico, C. Carfagna, A. Napolitano, M. d'Ischia, *Chem Commun (Camb)* **2011**, *47*, 10308.

[11] R. P. Zhang, Q. L. Fan, M. Yang, K. Cheng, X. M. Lu, L. Zhang, W. Huang, Z. Cheng, *Advanced Materials* **2015**, *27*, 5063.

[12] N. Hylton, *J Clin Oncol* **2006**, *24*, 3293; K. A. Miles, T. Y. Lee, V. Goh, E. Klotz, C. Cuenod, S. Bisdas, A. M. Groves, M. P. Hayball, R. Alonzi, T. Brunner, *Eur Radiol* **2012**, *22*, 1430; J. M. Hudson, R. Williams, C. Tremblay-Darveau, P. S. Sheeran, L. Milot, G. A. Bjarnason, P. N. Burns, *Eur J Radiol* **2015**, *84*, 1650.

[13] J. P. O'Connor, A. Jackson, G. J. Parker, G. C. Jayson, *Br J Cancer* **2007**, *96*, 189.

[14] K. Turetschek, A. Preda, V. Novikov, R. C. Brasch, H. J. Weinmann, P. Wunderbaldinger, T. P. Roberts, *J Magn Reson Imaging* **2004**, *20*, 138; D. L. Longo, F. Arena, L. Consolino, P. Minazzi, S. Geninatti-Crich, G. B. Giovenzana, S. Aime, *Biomaterials* **2016**, *75*, 47; D. L. Longo, W. Dastru, L. Consolino, M. Espak, M. Arigoni, F. Cavallo, S. Aime, *Magn Reson Imaging* **2015**, *33*, 725.

[15] T. Sarna, W. Froncisz, J. S. Hyde, *Arch Biochem Biophys* **1980**, *202*, 304.

[16] S. Aime, M. Fasano, E. Terreno, C. J. Groombridge, *Pigment Cell Res* **1991**, *4*, 216; S. Ghiani, S. Baroni, D. Burgio, G. Digilio, M. Fukuhara, P. Martino, K. Monda, C. Nervi, A. Kiyomine, S. Aime, *Magn Reson Chem* **2008**, *46*, 471.

[17] I. A. Vitkin, J. Woolsey, B. C. Wilson, R. R. Anderson, *Photochem Photobiol* **1994**, *59*, 455.

[18] N. Oh, J. H. Park, *Int J Nanomedicine* **2014**, *9 Suppl 1*, 51.

[19] K. W. Chan, T. Yu, Y. Qiao, Q. Liu, M. Yang, H. Patel, G. Liu, K. W. Kinzler, B. Vogelstein, J. W. Bulte, P. C. van Zijl, J. Hanes, S. Zhou, M. T. McMahon, *J Control Release* **2014**, *180*, 51.

[20] S. Folli, A. Pelegrin, Y. Chalandon, X. F. Yao, F. Buchegger, D. Lienard, F. Lejeune, J. P. Mach, *International Journal of Cancer* **1993**, *53*, 829.

[21] S. V. Hudson, J. S. Huang, W. Yin, S. Albeituni, J. Rush, A. Khanal, J. Yan, B. P. Ceresa, H. B. Frieboes, L. R. McNally, *Cancer Res* **2014**, *74*, 6271; J. Levi, S. R. Kothapalli,

S. Bohndiek, J. K. Yoon, A. Dragulescu-Andrasi, C. Nielsen, A. Tisma, S. Bodapati, G. Gowrishankar, X. Yan, C. Chan, D. Starcevic, S. S. Gambhir, *Clin Cancer Res* **2013**, *19*, 1494; R. Zhang, D. Pan, X. Cai, X. Yang, A. Senpan, J. S. Allen, G. M. Lanza, L. V. Wang, *Theranostics* **2015**, *5*, 124.

## Figures

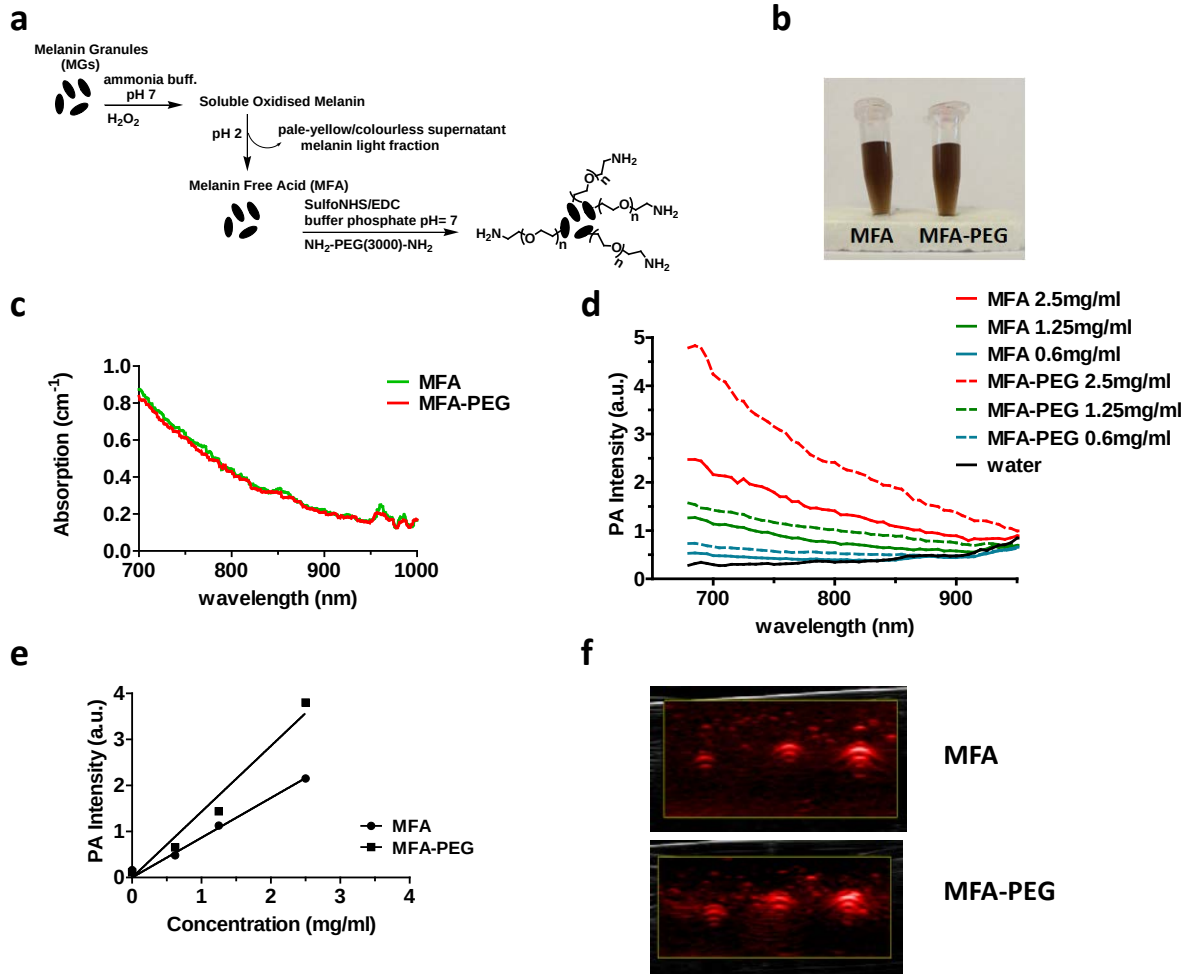


**Figure 1.** Schematic representation of the synthesis of MFA and MFA-PEG (a). Pictures of MFA and MFA-PEG solutions (2.5 mg/ml) dissolved in $H_2O$ after 4 months of storage in dark conditions at 4°C (b). UV-vis absorption (c) and PA spectra (d) of MFA and MFA-PEG in 1x PBS at pH=7.4. PA intensities as a function of MFA and MFA-PEG concentration in PBS (e). Representative PA images of MFA and MFA-PEG solutions in the range of concentrations 0.625 - 1.25 – 2.5 mg/ml each excited by pulsed laser at 700 nm (f).

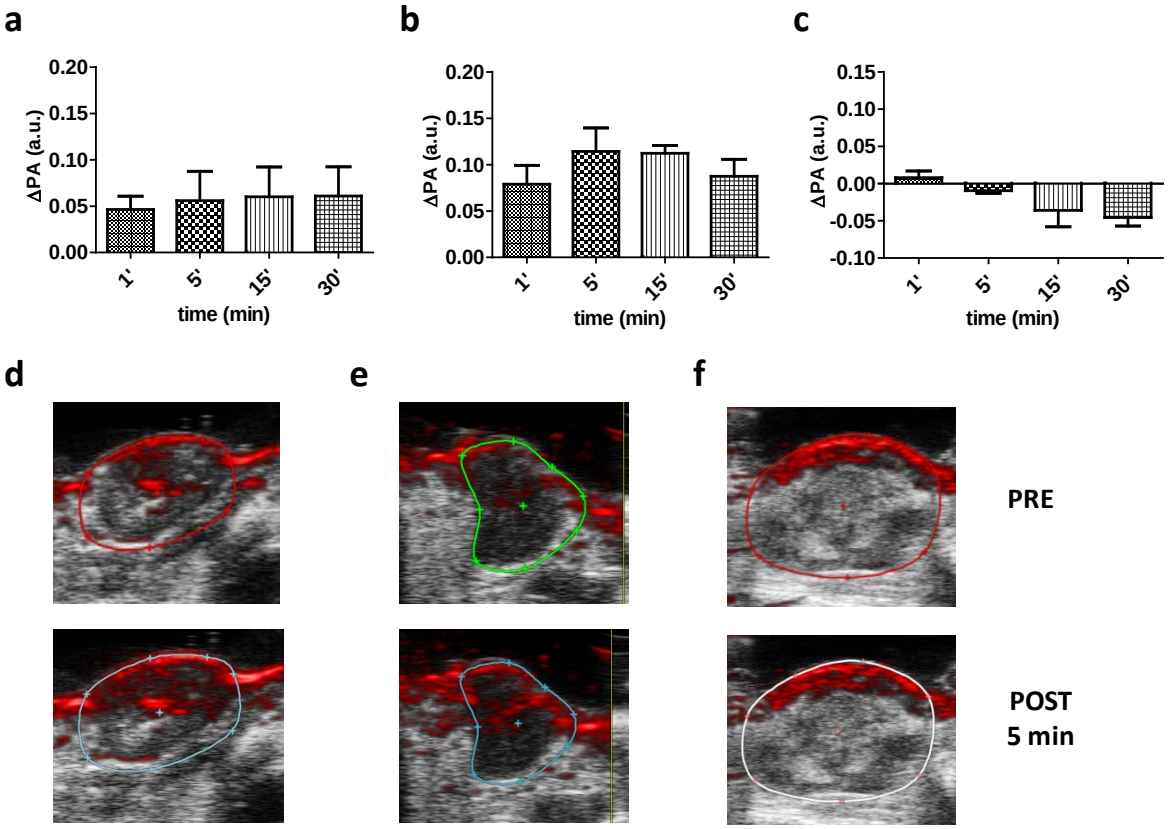


**Figure 2** Average PA signal changes upon intravenous administration of 0.1 mL of MFA (a) and MFA-PEG (b) with concentration of 2.5 mg/mL or of 0.1 ml PBS solution (c) in breast tumor bearing mice (n=4) at 700 nm. Representative optoacoustic images in transverse section of tumor before and 5 min after intravenous injection of MFA (d), MFA-PEG (e) and PBS (f) at 700 nm. All data are expressed as mean ±SD.

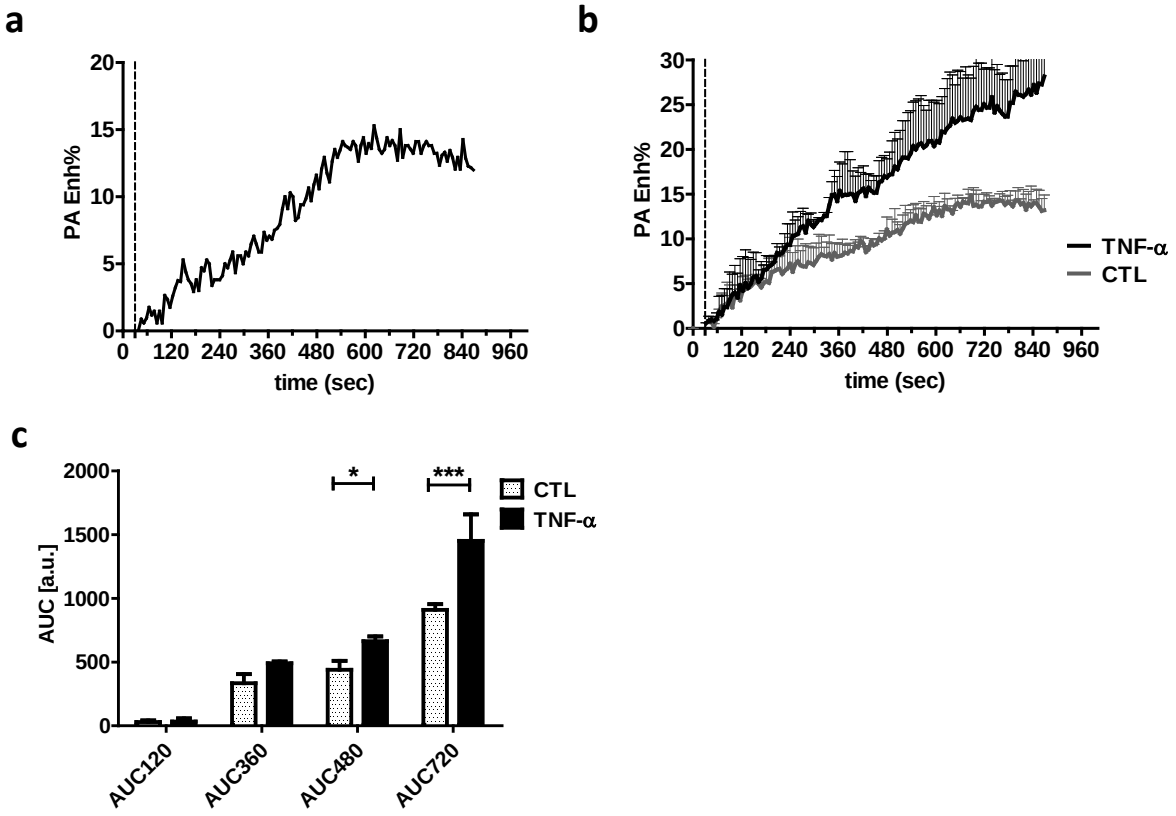


**Figure 3** Typical time PA intensity curve for intravenous bolus injection of 80 µL of MFA-PEG (2.5 mg/mL) in the tumor region (a). Averaged dynamic contrast enhanced PA curves (PA Enh%) upon MFA-PEG tail vein injection for control group (n=3) and for TNF-α treated group (n=4) (b). Area under the curve (AUC) values at different time points calculated on the corresponding dynamic contrast enhanced curves for control and TNF-α treated mice.

**The table of contents entry**

Dario L. Longo, Rachele Stefania, Chiara Callari, Francesco De Rose, Riccardo Rolle, Laura Conti, Lorena Consolino, Francesca Arena, Alexander A. Oraevsky and Silvio Aime*

**Water Soluble Melanin Derivatives for Dynamic Contrast Enhanced Photoacoustic Imaging of Tumor Vasculature and Response to Antiangiogenic Therapy**

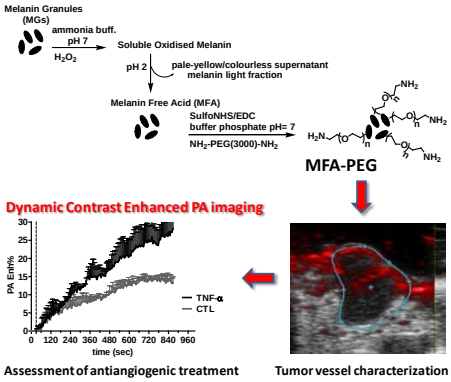


A dynamic contrast enhanced (DCE) approach for tumor photoacoustic (PA) imaging is described. Novel water soluble melanin-based derivatives are synthesized that exhibit good PA properties, stability, safety and accumulation in tumor bearing mice. This melanin derivative is capable to characterize tumor vasculature and to monitor vessel permeability changes upon anti-angiogenic treatment. This study demonstrates that DCE approaches are suitable for PA imaging for assessing the functional response to cancer treatments.

# Supporting Information

## Water Soluble Melanin Derivatives for Dynamic Contrast Enhanced Photoacoustic Imaging of Tumor Vasculature

By *Dario L. Longo, Rachele Stefania, Chiara Callari, Francesco De Rose, Riccardo Rolle, Laura Conti, Lorena Consolino, Francesca Arena,* and *Silvio Aime**

### Experimental Section

*Synthesis of MFA*

300 mg of synthetic melanin (sMG) were treated for 20 min at 30 °C under stirring with freshly prepared bleaching solution (0.2 ml per mg of melanin), by mixing stock solutions of ammonia (solution A) and hydrogen peroxide (solution B) in the 1:1 v/v ratio. Solution A was composed of $NH_3$ (3.00%), EDTA · 4Na · 2H2O (0.05%), and $H_2O$ (96.95%); solution B was composed of $H_3PO_4$ (1.76%), 30% $H_2O_2$ (9.40%), and $H_2O$ (88.84%). EDTA was added to solution A to remove chelated iron ions during the reaction of melanin synthesis. The obtained solution was treated with concentrated HCl to lower the pH to ~2. After two hours, the brown-black precipitate (Melanin Free Acid, MFA) was separated by centrifugation (3000 rpm for 5 min) from the supernatant and washed several times with $H_3PO_4$ 10 mM. MFA was finally dried in vacuum obtaining 143 mg of dark powder (yield 47%).

*Synthesis of MFA-PEG3000*

10 mg of MFA were dissolved in 2 ml of 0.1 M buffer phosphate solution (pH 6.6) and SulfoNHS (N-hydroxysulfosuccinimide) (26 mg). EDC (N-(3-dimethylamminopropyl)-ethylcarbodiimide hydrochloride) (28 mg) was dissolved in 400 µl of buffer and added to the MFA solution under stirring. A great excess of $H_2N\text{-}PEG_{3000}\text{-}NH_2$ (150 mg) in 1 ml of

phosphate buffer was added and the mixture was stirred overnight at room temperature. Purification of product by unattached PEG was performed by gel-filtration chromatography on a Superdex 200 10/300 GL column equilibrated with 10 mM sodium phosphate containing 150 mM NaCl (pH 7.2) on a FPLC Akta Purifier 100. The purified fraction containing MFA-PEG was collected and freeze-dried. The black-brown solid obtained was dissolved in 2 ml of bidistilled water and desalted using a PD10 column. $^{1}$H NMR spectroscopy analysis was performed by dissolving 1 mg of MFA-PEG in 600 µl of $D_2O$ and in 50 µl of sodium 3-(trimethylsilyl) propionate-2,2,3,3-d4 (TSP) 5 mM. The number of PEG chains per MFA was determined to be 3 from the ratio of peak area of $–OCH_2CH_2$-$PEG_{3000}$ group at 3.65 ppm and of $–CH_3$ TSP group at 0 ppm.

*Synthesis of MFA-$PEG_{3000}$-Cy5*

To a solution of Cy5 (S-07186) (50mg, 0.07 mmol) in dimethylacetamide (3 ml) were added NHS (20 mg, 0.17 mmol) and EDC (26 mg, 0.13 mmol) under stirring at room temperature for 3 h. The mixture was then added to a solution of $H_2N$-$PEG_{3000}$-$NH_2$ (0.15mmol, 460 mg) in DMA (6 ml); then 100 µl of N,N-diisopropylethylamine was added and stirred for 24 h at room temperature. The product was precipitated in 25 ml of diethyl ether, and then was dried under reduced pressure and used without further purifications. 1.5 mg of MFA in phosphate buffer (0.1M, pH 6.5, 1 ml) was cooled to 0 °C and EDC (2 mg, 10 mmol) and sulfoNHS (2 mg, 10 mmol) in phosphate buffer (0.5 ml) were added. The mixture was allowed to stir for 1 h. Then Cy5-$PEG_{3000}$-$NH_2$ (14.0 mg, 3.9 mmol) was added and the mixture was stirred overnight. Purification of product by unattached Cy5-PEG was performed by gel-filtration chromatography on a Superdex 200 10/300 GL column equilibrated with 10 mM sodium phosphate containing 150mM NaCl (pH 7.2) on a FPLC Akta Purifier 100. The purified fraction contains MFA-$PEG_{3000}$-Cy5 was collected and freeze-dried, dissolved in 1 ml of bidistilled water and desalted using a PD10 column.

*Stability of MFA and MFA-PEG*

Long-term stability of MFA and MFA-PEG in water (0.5 mg $ml^{-1}$) was assessed by measuring the hydrodynamic size up to 90 days of storage at 4°C. In addition, physiological stability of MFA and MFA-PEG (0.5 mg $ml^{-1}$) was assessed in cell culture medium (DMEM) and in a serum solution (10% fetal bovine serum, FBS, in PBS) after incubation at 37 °C for 24 h. Absorption values and PA images at 700nm were collected at 0 h, 2 h, 4 h and 24 h.

*Cytotoxicity assay*

The viability and proliferation of J774 macrophagic cells were evaluated by methyl thiazolyl tetrazolium (MTT) assay. Typically, J774 cells were incubated in the culture medium (DMEM) at 37 °C in an atmosphere of 5% CO2 and 95% air for 24 h. Subsequently, the culture medium was removed. The cells were incubated in culture medium containing MFA and MFA-PEG with different concentrations for another 24 h and washed with medium twice. 100 μl of the new culture medium containing MTT reagent (10%) was added to each well of the 96-well assay plate and incubated for 4 h to allow the formation of formazan dye. After removal of the medium, the purple formazan product was dissolved with DMSO for 15 min. Finally, the optical absorption of formazan was measured at 570 nm by iMARK microplate reader (Bio-Rad).

*Mouse Models*

BALB/c mice (Charles River Laboratories) were maintained at the Molecular Biotechnology Center, University of Turin and treated in accordance with University Ethical Committee and European guidelines under Directive 2010/63. All animal experiments were performed in compliance with the Guidelines for the Care and Use of Research Animals established by our University Animal Studies Committee. Murine breast cancer HER2+ cells (TS/A) suspended

in 100 µl of PBS were inoculated subcutaneously in the shoulder of 4−6 weeks old female BALB/c mice. When the tumors reached 0.5−0.8 cm in diameter, the tumor bearing mice were subjected to PA imaging studies.

*Biodistribution and Ex Vivo Tissue Analysis*

Optical imaging was performed with the IVIS 200 small animal imaging system (PerkinElmer). A customized filter set, exciting at 640 nm and acquiring at 680 nm, was used for data acquisition. Identical illumination settings (f-stop/field of views/binning/acquisition time, 2/12.8/8/1 s) were used to acquire all the images, and fluorescence emission was normalized to average radiance ($p \cdot s^{-1} cm^{-2} sr^{-1}$). Images were acquired and analyzed with Living Image Software 3.0.4 (PerkinElmer). Mice bearing TS/A subcutaneous tumors were injected intravenously with 20 µl of 0.06 mM MFA-PEG-Cy5 solution, anesthetized with 2.5% isoflurane (Abbott Laboratories) and then analyzed with the IVIS 200 after 5-10-15-20-30 min, 2 and 4 h. After 4 h mice were sacrificed for *ex vivo* biodistribution studies. Explanted organs were cleaned from surrounding tissue, washed in PBS placed on a piece of laboratory film and analyzed with the IVIS 200.

*PA Imaging of Phantoms*

Different concentrations of MFA and MFA-PEG aqueous solutions ranging from 0.625 to 5 mg $ml^{-1}$ were filled into polyethylene capillaries and then the capillaries were laid on the surface of solidified 1% agarose gel. The capillaries were further covered with thin 1% agarose gel to make the surface smooth. The VevoLAZR PA imaging system (VisualSonics Inc., Toronto, Canada) with a laser at excitation wavelengths in the range 680 to 970 nm with 5 nm step and a focal depth of 10 mm was used to acquire PA and ultrasound images. Stability experiments were carried out with the with the LOIS-3D Laser Optoacoustic Imaging System (Tomowave Systems, Houston TX), equipped with a q-switched Nd:YAG

pumped Ti:Sapphire laser (Quanta Systems, Solbiate Olona, Italy) with laser pulse set to 700nm. Optoacoustic images were acquired by rotating the phantoms 360 deg submerged in degassed distilled water at constant temperature of 30°C.

Image analysis was carried out using the respective proprietary software. Briefly, quantification analysis was performed on the PA images with ROIs drawn over the sample on the PA images.

*PA Imaging of Tumor Bearing Mice*

Mice bearing TS/A tumors were anesthetized with 1-2% isoflurane in oxygen then depilated using a combination of shaving and application of nair cream (Veet), which was removed with moist gauze. Anesthetic depth was maintained throughout the image acquisitions, with mice oriented ventral side up in the animal holder and body temperature was monitored continuously with a rectal thermometer and kept at 37°C. PA imaging was performed using the same VevoLAZR PA system as for the in vitro study. MFA (2.5 mg/ml), MFA-PEG (2.5 mg $ml^{-1}$) and saline solutions were administered intravenously through the tail vein in a volume of 100 μL. Quantification analysis of PA signals was performed on the PA images by subtracting images recorded at 700 nm at several time points (1, 5, 15 and 30 minutes) post-injection to the PA signal intensity before the injection.

*Dynamic Contrast Enhanced (DCE)-PA Imaging*

Mice bearing TS/A tumors were photoacoustically imaged 3 h after tail vein administration of 100 μl of TNF-α at 10 μg/ml (n=4, TNF-α treated) or of 100 μl of saline solution (n=3, control) using the same VevoLAZR PA system as for the in vitro study. Mice were anesthetized with 2% isoflurane in oxygen and placed in lateral position. 2D PA images passing throughout the central tumor region were acquired by exciting at 700 nm with a sampling rate of ca. 6s. Images were acquired before (30s of baseline acquisition) and after

intravascular tail vein injection of 80 μL of MFA-PEG (2.5 mg $ml^{-1}$) for 15 min. The mean PA intensity along the first 30s images before contrast injection was defined as the pre-contrast PA signal baseline ($PA_{pre}$). PA signal enhancements were calculated at each time point of the dynamic scan, according to Eq. [1]:

$$PAenh(t) = \frac{\left(PA(t) - PA_{pre}\right)}{PA_{pre}}$$

where in each voxel PA(t) is the PA intensity at time point t. The area under the PA enhancement curve (AUC) was calculated integrating the PA enhancement curve at several time points (120, 360, 480 and 720 s) using the trapezoidal rule. Mean AUC values were calculated within the tumor region for each group.

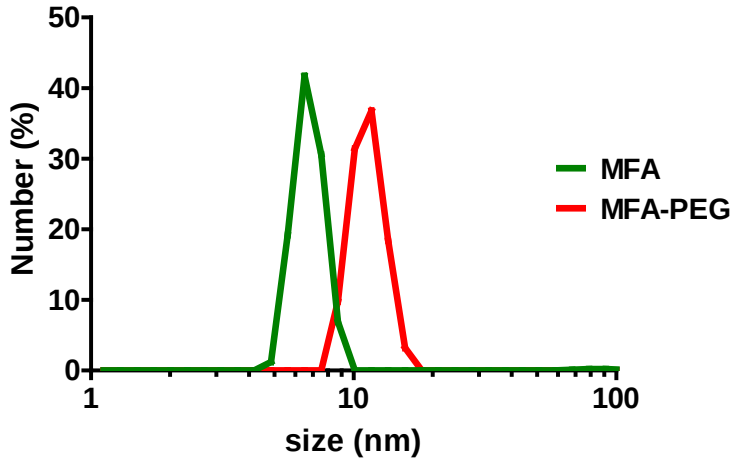


**Figure S1.** Representative DLS diagram of MFA and MFA-PEG.

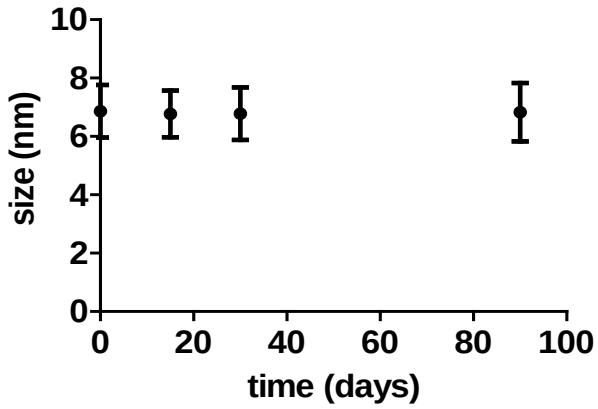


**Figure S2.** DLS data of MFA (0.5 mg/ml) after storage at 4°C under dark over a period of 3 months.

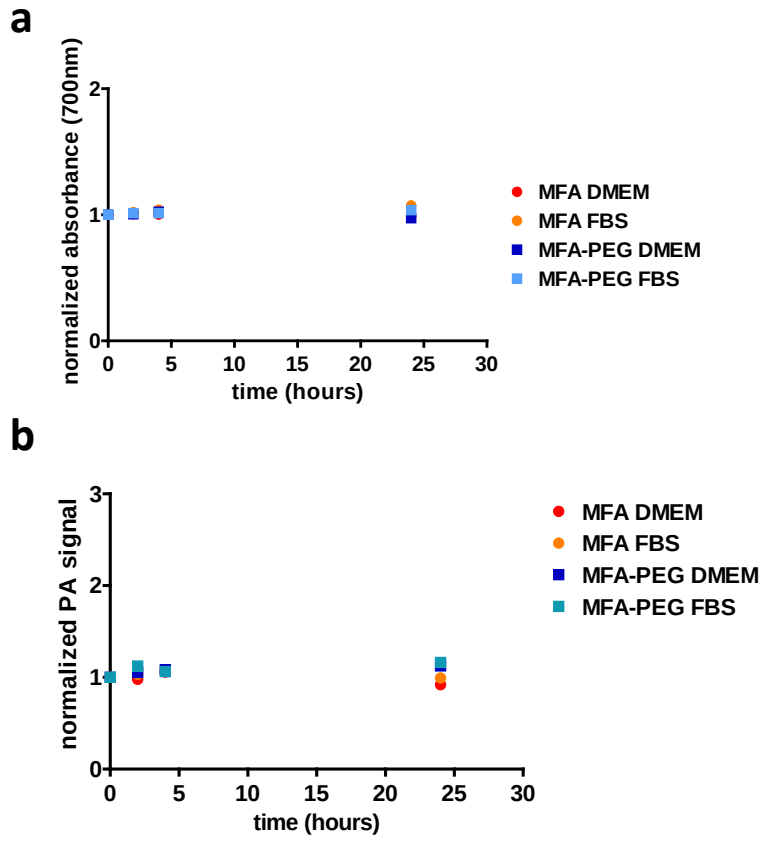


**Figure S3.** Normalized absorbance and PA signal intensities of MFA and MFA-PEG (0.5 mg/ml) dissolved in cell culture medium (DMEM) or in serum (10% fetal bovine serum) after 2, 4, and 24h in comparison to freshly prepared solutions.

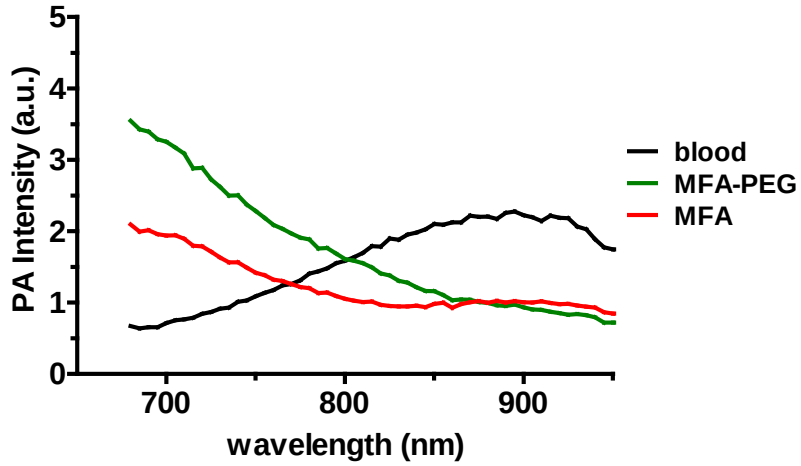


**Figure S4.** PA signal intensities of MFA and MFA-PEG (1.25 mg/ml) in presence of full blood.

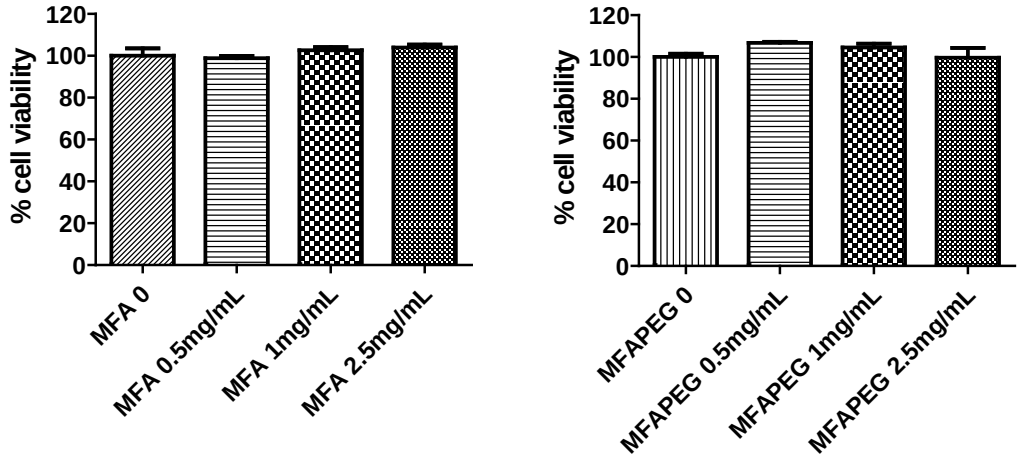


**Figure S5.** Cytotoxicity studies of MFA (a) and MFA-PEG (b). In vitro viability of J774 macrophagic cells treated with MFA and MFA-PEG solutions at concentrations of 0.5, 1.0 and 2.5 mg/ml for 24h. The percentage of cell viability of treated cells was calculated relative to that of cells treated with the same volume of PBS. Error bars represent standard deviation of three independent experiments, each performed in triplicate.

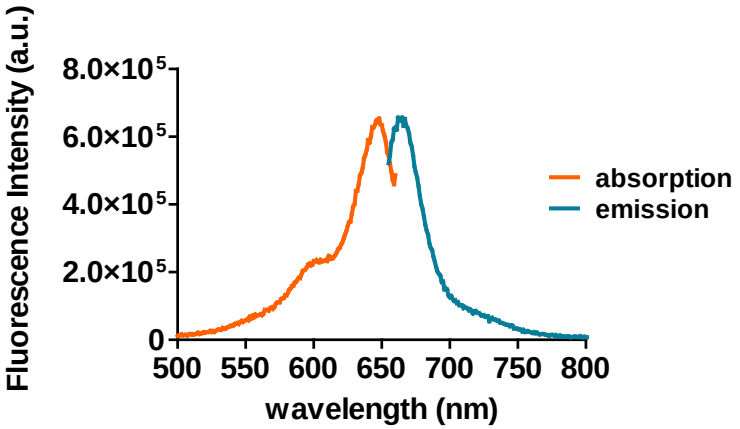


**Figure S6.** Absorption and emission spectra for the fluorescent MFA-PEG derivative (MFA-PEG-Cy5).

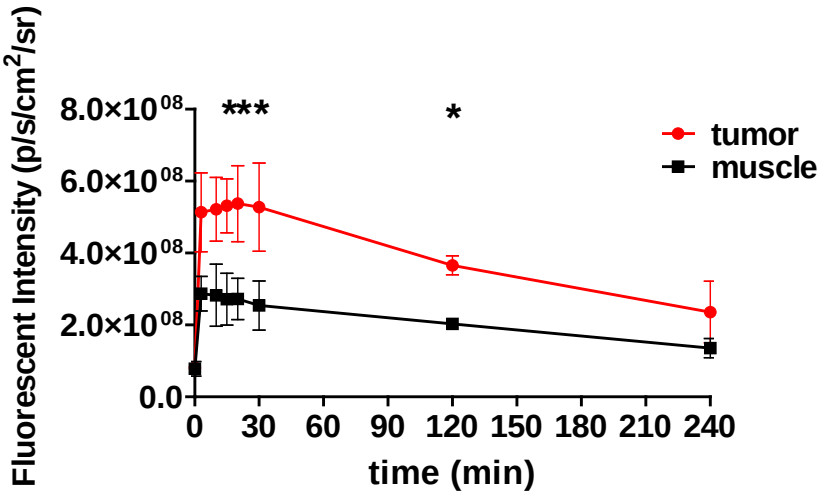


**Figure S7.** Mean fluorescence intensity in the tumor and muscle regions of interest (ROIs) as a function of time after intravenous injection of 20 µL of 0.06 mM MFA-PEG-Cy5 solution.

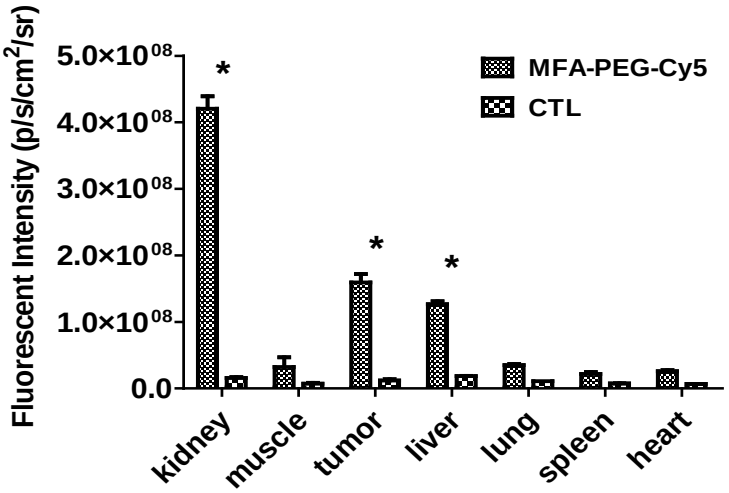


**Figure S8.** Fluorescence intensity (mean ± SEM) of several tissues explanted from mice sacrificed 4 h after intravenous injection of 20 μL of 0.06 mM MFA-PEG-Cy5 solution or of PBS (CTL).